IOP Conference Series:
Earth and
Environmental Science

PAPER • **OPEN ACCESS**

Comparison of the reliability of strength limit calculation methods for prismatic samples with different spreading of normal contact stresses in their wedge failure shape

To cite this article: Leonid Vasyliev *et al* 2024 *IOP Conf. Ser.: Earth Environ. Sci.* **1348** 012033

IOP Conf. Series: Earth and Environmental Science **1348** (2024) 012033 doi:10.1088/1755-1315/1348/1/012033

Comparison of the reliability of strength limit calculation methods for prismatic samples with different spreading of normal contact stresses in their wedge failure shape

Leonid Vasyliev[1], Dmytro Vasyliev[1], Mykola Malich[1], Zakhar Rizo[1,2] and Denys Kress[1]

[1]M.S. Poliakov Institute of Geotechnical Mechanics of the National Academy of Sciences of Ukraine, Simferopolska St., 2a, Dnipro, 49005, Ukraine

[2]Corresponding author: zaharrizo777@gmail.com

Abstract. This article explores methods for calculating the strength limits of solid objects subjected to compression. Traditionally, two stress distribution patterns are used: the exponential pattern by E.P. Unksov and the linear pattern by L. Prandtl. The authors introduce an enhanced stress distribution method. They compare the accuracy of these methods in calculating strength limits and constructing "normal stress - longitudinal strain" diagrams for wedge-shaped failures in rock samples. Four properties are considered: shear strength, coefficients of internal and external friction, and elasticity modulus. The results show that, with an external friction coefficient up to 0.3, all methods yield similar accuracy in strength limit calculations and ultimate stress-strain curves. Some curves exhibit stress drops, explained by a transition from convex to concave slip lines during failure. Additionally, there are hardening curves in the ultimate curves without theoretical justification. The comparison of calculated strength limits with experimental data confirms the method's accuracy: 13.7% error for the exponential method, 11.4% for the linear method, and 8.1% for the enhanced distribution, especially for low contact friction values (up to f_c=0.3).

1. Introduction

The authors of the article have developed several methods for calculating strength limits and parameters of stress-strain diagrams for prismatic specimens based on the theory of slip lines, applied to some of the known forms of failure according to L.I. Baron. In some cases, they employed the exponential distribution law of normal contact stresses (σ_{yi}, Pa) according to the formula

$$\sigma_{y_i} = \sigma_{y0} \exp\left(\frac{2 f_c \cdot x}{h}\right), \quad (1)$$

In other cases, they employed the linear distribution according to L. Prandtl [1], following the formula

$$\sigma_{y_i} = \sigma_{y0}\left(1 + \frac{2 f_c \cdot x}{h}\right), \quad (2)$$

where σ_{y0} – the vertical normal stress at the corner point of the specimen, Pa; f_c– coefficient of friction; x – the abscissa of the studied point on the specimen, m; h – the height of the specimen, m.

Both of these expressions have been derived by the authors from the joint solution of one ordinary differential equation and one algebraic equation. In solid mechanics, there is a recommendation that, when solving the stress-strain state of a body under plane deformation, the conditions for the joint solution of two partial differential equations should be satisfied at any point of the body [1]

$$\frac{\partial \sigma_x}{\partial x} + \frac{\partial \tau_{xy}}{\partial y} = 0; \tag{3}$$

$$\frac{\partial \sigma_y}{\partial y} + \frac{\partial \tau_{xy}}{\partial x} = 0, \tag{4}$$

where σ_y, σ_x, τ_{xy} – vertical and horizontal normal and tangential stresses in the specimen body, Pa; and one algebraic equation of equilibrium [1, 2, 3].

$$\sigma_x = 2\sqrt{k^2 - \tau^2_{xy}}, \tag{5}$$

where k – material resistance to pure shear, Pa.

To meet the requirements of solid mechanics, the authors of this article [2] have developed a theoretically more accurate law for the distribution of contact stresses based on the solution of the mentioned equations (3) - (5) for rock materials.

From the solution, the relationship of derivatives in the form [formula] is obtained:

$$\frac{\partial \sigma_x}{\partial x} = \frac{2 f_c \sigma_y}{h} + \left[\frac{2\mu}{\cos\rho} \left(\sin\rho - \sqrt{1 - b_\xi^2} \right) + \left(\frac{2 b_\xi (f_c - \mu)}{\cos\rho \sqrt{1 - b_\xi^2}} \right) \right] \frac{\partial \sigma_y}{\partial y}, \tag{6}$$

where σ_y – vertical normal stress, Pa; $\mu = \mathrm{tg}\rho$ – coefficient of internal friction and ρ – angle of internal friction, rad;

$$b_\xi = \frac{f_c \sigma_y}{k + \mu \sigma_y} \tag{7}$$

Let's denote the expression in square brackets in (6) formula as g. Then the expression (1) given the coefficient g for the prism of the unit width based on equations (3) and (4) has the form:

$$\sigma_{y_i} = \sigma_{y0} \exp\left(\frac{4 f_c \cdot x}{gh} \right). \tag{8}$$

Let's expand the formulas for calculating the specific pressure corresponding to this condition, where $x > 0.5a_1$
with $x > 0.5a_1$

$$p = \sigma_y \frac{gh}{2 f_c} \left(\exp\left(\frac{4 f_c \left(a_1 - x_a + \cdot x_d \right)}{hg} \right) - 1 \right) \Big/ \left(x_a + x_d \right) \tag{9}$$

with $x < 0.5a_1$

$$p = \sigma_y \frac{h}{2 f_c} \left(\exp\left(\frac{2 f_c \left(a_1 - x_a + \cdot x_d \right)}{h} \right) - 1 \right) \Big/ \left(x_a + x_d \right), \tag{10}$$

where with $x \le 0.5a_1$ $x_a = x$; with $x \ge 0.5a_1$ $x_a = a_1 - x_d$; where x_d – the initial fixed value of the abscissa

can be translated to English as "initial fixed abscissa value *x*.

However, a comparison of the accuracy in calculating the strength limit using these three distributions has not been conducted.

Let's take, for example, one of the most complex forms of failure - wedge-shaped failure. Unlike the other four forms of failure, wedge-shaped failure involves a crack that intersects the vertical line of symmetry and attaches to a detached triangular piece in the contact area. Therefore, the aim of this study is to determine the level of accuracy in calculating the strength limits using the exponential distribution (according to Unksov), linear distribution (according to Prandtl), and the author's distribution of contact normal stresses.

2. Methods

Let's clarify the assumptions outlined in [1]. There, the side walls of the specimen are assumed to be straight. In real conditions, due to deformation, the walls have a barrel-like shape (figure 1). During deformation, the shape of the body is distorted. We neglect the distortion of the cross-sectional shape inside the rock specimen. However, in the corner regions of the specimen, we take into account the rule of tangential stress pairings because, due to deformation, the specimen acquires a barrel-like shape, as reflected in figure 1. In this new diagram, an adjustment is made to the distribution of contact loads. We consider the deformation process at each moment to obtain results that correspond to the entire period of the failure process. We place the origin of the coordinate axes in the upper-left corner of the specimen. The y-axis points downward, i.e., in the direction of the applied force, and the x-axis runs along the contact plane from left to right. Friction forces are directed against transverse deformation, from the edges of the specimen toward the vertical plane of symmetry of the specimen. According to the sign convention, tangential stresses from friction in the upper-left quarter of the figure are taken as positive, while in the right quarter, they are negative. In the lower quarters, the stresses have opposite signs accordingly. We assume that tangential stresses from friction along the height of the specimen decay linearly. Along the horizontal line of symmetry, they have zero values.

Now let's discuss the conditions for the development of cracks (figure 1).

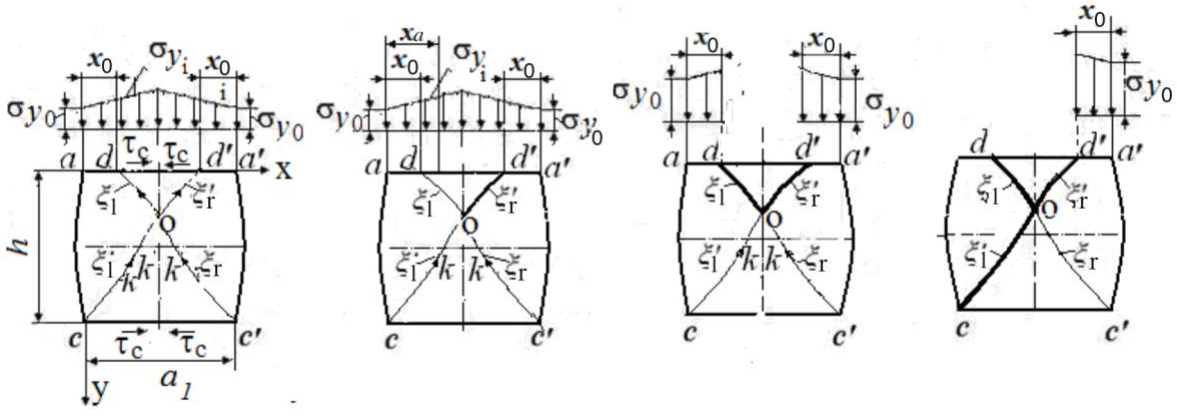

Figure 1. Diagram illustrating the formation of a wedge-shaped failure in a rock specimen during compression: a) at the moment of failure limit; b) at the moment of the right side of the wedge formation; c) at the moment of the left side of the wedge formation; d) at the moment of wedge formation**,** ξ_l – left slip line; ξ_r – right slip line (SL).

According to the theory of slip lines, cracks can propagate from top to bottom and from bottom to top. Considering the top-down perspective is more speculative. It is clear that the crack initiation process begins at the SL at the point where the least stress is required for its formation.

Let's assume that the distribution of contact normal stresses has the shape shown in the diagram,

in this case, following E.P.Unksov's pattern. According to L. Prandtl, the loading scheme is similar, but instead of an exponential distribution, it has a triangular shape. Let's imagine that a crack forms at a point *d*' on the right SL ξ'_r, conjugated with SL ξ'_l, exiting from the bottom-left corner on the exposed surface of the specimen. During the fracture process, exposure plays a crucial role. Therefore, the condition for the crack to exit at the lower corner point in the wedge-shaped failure is a regular occurrence. In principle, the problem can also be solved with fracture initiation in the left half of the specimen. The solutions are equivalent, but there are some non-essential differences in the signs of SL parameters. As the crack develops, a portion of the specimen is relieved from the load, determined by the projection of the crack surface onto the horizontal plane. By knowing the coordinates of the vertex of one or two cracks at each moment, it is possible to determine the load-bearing portion of the specimen, which is equal to the initial unit length minus the part relieved from the load. The part relieved from the load can be easily determined based on the geometry of SL. With knowledge of the ultimate average loads on the load-bearing portion of the specimen, the deformation magnitude can be determined using Hooke's law. Since the crack in the examined case develops along two different SL ξ'_r and ξ'_l two vertical halves of the specimen from right to left, we will describe its conditions of development and the regularities of specific forces in abscissa $x \geq 0.5a_l$ and $x \leq 0.5a_l$ in separateness, where a_1 – specimen width, m.

At the same time, it should be taken into account that when the right part of the crack develops, the left part of the sample will be under a specific load, Pa

$$p = \int_0^{0.5a_1} \sigma_{y0} \cdot \varphi(x)dx \Big/ 0.5a_1 , \tag{11}$$

and the right one is under load, Pa

$$p = \int_0^{0.5a_1} \sigma_{y0} \cdot \varphi(x)dx \Big/ (x_a + x_0) , \tag{12}$$

where $\varphi(x)$, Pa – the function of the increment of normal stress on a unit contact surface of the specimen that has not been relieved from the load; $x_a=a_1-x$, *m*.

When stress is distributed according to E.P. Unksov, expression (4) takes the following form:
with $x \geq 0.5a_l$

$$p = \sigma_{y0} \frac{h}{2f_c}\left(\left(\exp\left(\frac{f_c a_1}{h}\right)-1\right)+\exp\left(\frac{2f_c(x_a-0.5a_1+x_0)}{h}\right)-1\right)\Big/(x_a+x_0) ; \tag{13}$$

with $x \leq 0.5a_l$

$$p = \sigma_{y0} \frac{h}{2f_c}\left(\left(\exp\left(\frac{f_c x}{h}\right)-1\right)+\exp\left(\frac{2f_c x_0}{h}\right)-1\right)\Big/(x+x_0) \tag{14}$$

When stress is distributed according to L. Prandtl, expressions (10) and (11) have *a* simpler form:
with $x \geq 0.5a_l$, m

$$p = \sigma_{y0}\left((x_a+x_0)+(x_a+x_0)\frac{2f_c}{h}+\left(0.5a_1+0.25a_1\frac{2f_c}{h}\right)\right)\Big/(x+x_0) ; \tag{15}$$

with $x < 0.5a_l$, m

$$p = \sigma_{y0}\left(\left(x+\frac{f_c}{h}x^2\right)+\left(x_0+\frac{f_c}{h}{x_0}^2\right)\right)\Big/(x+x_0) . \tag{16}$$

Here, it is necessary to clarify regarding the longitudinal normal stress σ_{y0} (Pa) at the top of the crack. Stress σ_{y0} with a value of zero relates to the entire specimen. At the moment of crack formation, the zero symbol is replaced with the symbol corresponding to the respective SL along which the crack is propagating. As seen from equations (10) - (13), the first thing to determine is the value of normal stress σ_y (Pa) at the corner point, or more precisely, at the crack tip.

Clearly, analytical methods should be based on *a* strength criterion that best describes the processes of deformation and failure in rock materials. We rely on *a* variety of the classical, third theory - the theory of maximum effective tangential stresses - *a* theory based on Coulomb's criterion [1]. Due to its good convergence with experimental data, this criterion is widely used in the theory of stress states of granular materials, soils, and the mechanics of rock materials [3-15]. It should be noted that in literature [3-8,9-15], there is still no universally accepted strength criterion. We have improved Coulomb's criterion by taking into account contact friction. This improvement allowed us to develop a new theory of local failure in rock materials [1], which enables the determination of stresses at any point within a deformable body, primarily at the crack tip and the parameters of its geometry. The reader will later see the effectiveness of our improvement.

Coulomb's criterion for cohesive materials is based on the assumption that the shear resistance of the rock is τ_α (Pa) on the considered surface is equal to the sum of the resistance to pure shear k_n (Pa) and a value proportional to the normal stress σ_α (Pa) on this site (the compression is positive),

$$\left|\tau_\alpha\right| = k_n + \mu\sigma_\alpha \tag{17}$$

or

$$k_n = \left|\tau_\alpha\right| - \mu\sigma_\alpha, \tag{18}$$

where k_n– material shear resistance limit, Pa; μ– the coefficient of internal friction; ρ –internal friction angle, rad.

This equality (16) should be understood as follows: failure will not occur if the left-hand side is less than the right-hand side. This criterion limits the shear stresses in any direction, which is why it involves the absolute value of τ_α. Using this criterion, we derived formulas for calculating vertical stresses at the crack tip. Here, we present the final basic formulas without derivation. They are applicable for each form of failure with specific adjustments. The formulas for determining the value of the ultimate longitudinal normal stress at the crack tip have the following form [1]

$$\sigma_y = \frac{1}{\mu}\left[\frac{k_n\left(1+\sin\rho\sqrt{1-b^2{}_{\xi'r(l)}}\right)\exp\left(2\mu\left(\beta_{\xi'r(l)}+\beta_{o(c)}\right)\right)}{1-\sin\rho\sqrt{1-b^2_{o(c)}}} - k_{o(c)}\right], \tag{19}$$

where

$$k_{o(c)} = \frac{\left(k_n+\mu\sigma_y\right)\cdot\left(1-\sin\rho\sqrt{1-b^2_{o(c)}}\right)}{\left(1+\sin\rho\sqrt{1-b^2_{\xi'r(l)}}\right)\cdot\exp\left(2\mu\left(2\beta_{o(c)}\right)\right)}; \tag{20}$$

$k_{o(c)}$, Pa – effective shear stress at point *o* or at the point *c*; $\beta_{\xi'r(l)}$, rad – angle of rotation SL ξ'_r or SL ξ'_l at the top of the crack; $\beta_{o(c)}$, rad – angle of rotation SL ξ'_r and ξ'_l from contact friction at points *o* and *c*.

$$b_{\xi'\mathrm{r(l)}} = \frac{f_c\left(1-\frac{2y}{h}\right)\sigma_y(x)}{k_\mathrm{n}+\mu\sigma_y(x)}; \tag{21}$$

$$b_{0(c)} = -\frac{f_\mathrm{c}\cdot\sigma_y\left(x_{\mathrm{o(c)}}\right)}{k_{\mathrm{o(c)}}+\mu\sigma_y\left(x_{\mathrm{o(c)}}\right)}, \tag{22}$$

$\sigma_y(x)$, Pa – the function for the distribution of normal stresses on the contact surface; $x_{\mathrm{o(c)}}$ – the abscissa of the point where SL intersects the axis of symmetry at either point *o* or at the point where it exits to the specimen's surface.

Due to the fact that at the point *d*' (figure 1) The effective shear stress reaches the value of k_n, (Pa) – the crack forms at the field point of the material's shear resistance and then propagates along the path of maximum effective tangential stresses (along the slip line). Therefore, in equation (20), linear decay of tangential stresses due to external friction as one moves away from the contact surface is taken into account according to the expression $(1-2y)/h$. Point *o* for SL ξ'_r or point *c* for SL ξ'_l are committed. Therefore, the value of the shear stress from external friction is taken into account by the value of the abscissa x_o, (m) on the vertical axis of symmetry and at the point *c* with x=0 and $y = h$, (m). The minus and plus signs in expressions (1, 5) and (1, 6) indicate the different role of external friction on the contact planes.

Parameters $\beta_{\xi\mathrm{r(l)}}$ (rad) and $\beta_{\mathrm{o(c)}}$ (rad) are determined by equations

$$\beta_{\xi'\mathrm{r(l)}} = \frac{1}{2}\operatorname{arctg}\frac{b_{\xi_{\mathrm{r(l)}}'}\cos\rho}{\sin\rho-\sqrt{1-b^2_{\xi'r(l)}}}; \tag{23}$$

$$\beta_{\mathrm{o(c)}} = \frac{1}{2}\operatorname{arctg}\frac{b_{\mathrm{o(c)}}\cos\rho}{\sin\rho-\sqrt{1-b^2_{\mathrm{o(c)}}}}, \tag{24}$$

where $\beta_{\xi'\mathrm{r(l)}}$, (rad) – rotation angles SL ξ'_r or SL ξ'_l from contact friction at the top of the crack; $\beta_{\mathrm{o(c)}}$, (rad) – rotation angles SL ξ_o or SL ξ_c from contact friction at points *o* and *c*.

In addition, it should be noted that formulas (20) and (22) determine the parameters $b_{\xi_{\mathrm{r(l)}}}$, $\beta_{\xi_{\mathrm{r(l)}}}$ at the point of the horizontal line of symmetry, while formulas (21) and (23) determine the parameters b_o, β_o at the point on the vertical line of symmetry, which have zero values.

In conclusion, it should be noted that the inclination angles SL ξ'_r and ξ'_l (figure 1) are determined by the formula

$$\alpha_{\xi'\mathrm{r(l)}} = \frac{3\pi}{4}-\frac{\rho}{2}+\beta_{\xi'\mathrm{r(l)}}. \tag{25}$$

Using the specific force values obtained from equations (7) and (8), it is possible to construct a true stress-strain diagram (figure 2, line 1). To do this, it is necessary to correlate the specific force values with the specimen's deformation, determined by the formula

$$\varepsilon = \frac{p}{E}, \tag{26}$$

where E – coefficient of elasticity, Pa.

However, in the practice of deforming bodies, it is common to use conditional diagrams when relating the variable load-bearing area during the process of failure to the initial width of the specimen. This relationship is described by the formula

$$S= (x+x_o)/a_1, \quad (27)$$

where S, Pa – the relative area of the specimen.

By multiplying the deformation value according to expression (23) by the value of the relative area S (24), we obtain the relationship between the parameters of the conditional stress-strain diagrams for exponential and linear distributions according to formulas (9) and (10).

As can be seen, the system of equations (5–24) is explicitly unsolvable because some of the formulas are transcendental. Solving the equation to determine the strength limit of specimens using this system was performed by the iterative method.

3. Results and discussion

As a result of the research, an analytical method has been developed for constructing conditional stress-strain diagrams for wedge-shaped failure of prismatic samples of rock using four properties (k_n - shear strength of the material; f_c, μ - coefficients of contact and internal friction, E - modulus of elasticity) that are available for experimental determination in laboratories of production enterprises using simple technical means, without the need for complex, expensive presses, which are only available in Ukraine at the Institute of Geotechnical Mechanics of the National Academy of Sciences of Ukraine and the Krivyi Rih Technical University, far from consumers - production enterprises. Figure 2 shows stress-strain diagrams constructed at k=10 MPa, E=5500 MPa.

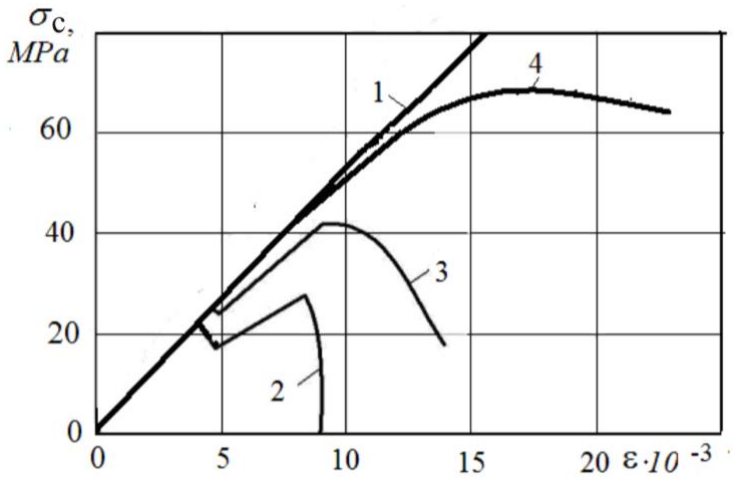

Figure 2. Stress-strain diagrams for wedge-shaped failure of prismatic samples: 1 - true stress-strain diagram; 2 - ρ=20°; f_c=0.3; 3- ρ=30°; f_c = 0.3; 4 - ρ=38°, f_c= 0.25.

The ultimate curves of theoretical diagrams (figure 2) correspond in appearance to the experimental ones [3]. Some of them exhibit stress drops, which are confirmed by experimental observations. At the moment of stress drop, so-called yield platforms appear, and the formation of these platforms is explained by the transition of the failure process from a convex slip line to a concave one, resulting in different characteristics of the ultimate curves. In the concluding section, the ultimate curves feature hardening curves that have not yet received theoretical justification. This phenomenon is explained by the transition of the failure process to a concave slip line, characterized by this particular attribute.

The determination of the strength limit of specimens under uniaxial compression is performed based on the maximum value of the ultimate curve.

Table 1 provides a comparison of calculated strength limits for exponential distribution (E.P. Unksov), linear distribution (Prandtl), and the refined distribution of contact normal stresses proposed by the authors.

Table 1. Comparison of calculated strength limits with experimental data, borrowed from the register of rock materials [16] for the wedge-shaped failure of prismatic specimens.

Type of rock	Experimental			Kadastr [p.16]	Calculation					
					By Unksov		According to Prandtl		Refined Values	
	k_n, MPa	ρ, grad	σ MPa		σ MPa	Coef var, %	σ MPa	Coef var, %	σ MPa	Coef var, %
Argillite	4.0	35	24.0	172	21.3	11.3	20.3	15.4	27	12.5
Sandstone	6.63	36	32.5	172	38.0	16.9	36.3	11.7	36	10.8
Hornfels	25.0	39	138.0	66	164	18.8	153.0	10.9	116	15.9
Argillite	7.85	35	46.5	172	39.9	14.2	39.2	15.7	46	1.1
Argillite	5.0	30	24.0	171	20.5	14.6	21.2	11.7	24	0
Aleurolite	6.5	31	35.0	174	27.9	20.3	27.6	21.1	32.5	7.1
Sandstone	10.0	30	55.0	158	41.0	25.5	40.8	25.8	48	12.7
Limestone	12.0	30	60.0	158	50.0	16.7	49.3	17.8	57	5
Hematized Magnetite	20.0	32	97.0	66	127	30.9	91.0	6.2	101	4.1
Hematized Tuff	25.0	36	134.0	67	127	2.2	136.9	2.2	154	14.9
Garnet-Magnetite Skarn	10.0	39	68.0	67	56.0	17.6	65.4	3.8	70	2.9
Hornfels with dense veins of magnetite and epidote	16.0	34	84.0	67	78.3	6.8	81.0	3.6	89	6.0
Quartz-Magnetite Ore	22.0	39	152.0	67	145.0	4.6	144.0	5.3	155	2.0
Mean values of the coefficient of variation	–	–	–	–	–	15.4	–	11.6	–	7.2

4. Conclusions

The comparison of calculated strength limits with experimental data confirmed the accuracy of the developed method for exponential distribution with an error of 15.4%, for linear distribution with an error of 11.6%, and for the refined distribution proposed by the authors with an error of 7.2%. This indicates their sufficient accuracy for practical purposes at low values (up to fc=0.3) of contact friction. It is reasonable to assume that at high values of contact friction, the accuracy of calculations for exponential distribution may decrease due to the increasing sharpness of these distributions.

References

[1] Vasiliev L M Vasiliev D L Malich N G and Angelovskiy A A 2018 *Mechanics of formation of deformation shapes in rock samples under compression: a monograph* IMA-press

[2] Vasiliev L M Zhuravkov M A Vasiliev D L Malich N G and Nazarov A E 2020. Improvement of the compression strength calculation method. *Mechanics of Machines, Mechanisms, and Materials* 4 85-91

[3] Litvinskiy G G 2008 *Analytical theory of the strength of rocks and massifs* (Donetsk: Nord-Press)

[4] Petrenko V D Tyutkin O L and Kulazhenko Y Y 2014 The problem of determining deformations of the lining of bend tunnels with significant changes in engineering and geological conditions *Collection of Scientific Works "Bridges and Tunnels*: *Theory, Research, Practice,*" DNURT (5) 62-69

[5] Petrenko V D Tyutkin O L Lubinchik, O I and Kildeev V R 2015. Assessment of stability of natural slopes using mathematical modeling in the "OTKOS" program. *Collection of Scientific Works of Dnipro University of Railway Transport "Bridges and Tunnels: Theory,*

Research, Practice" DNURT (8) 23-32
[6] Zhang L, Zhang P and Radha K 2010 Evaluation of rock strength criteria for wellbore stability analysis *International Journal of Rock Mechanics and Mining Sciences* **47**(8) 1304-1316
[7] Mingqing Y 2010 Mechanical characteristic of the exponential strength criterion under conventional stresses *International Journal of Rock Mechanics and Mining Sciences* **47**(2) 195-204
[8] Zhao X Cai M A 2010 mobilized dilation angle model for rocks *International Journal of Rock Mechanics and Mining Sciences* **47**(3) 368-384
[9] Feiying M, Yongqing W, Haitao L, Lin W, Hui W and Rui J 2014 Staged Coalbed Methane Desorption and the Contribution of Each Stage to Productivity *Chemistry and Technology of Fuels and Oils* **50**(4) 344-353
[10] Eberhardt E 2012 The Hoek–Brown Failure Criterion *Rock Mechanics and Rock Engineering* **45**(6) 981–988
[11] Agustawijaya D 2011 The Influence of Rock Properties and Size into Strength Criteria: A Proposed Criterion for Soft Rock Masses *Civil Engineering Dimension* **13**(2) 75-81